Method of choice for fabrication of high-quality ZnO-based Schottky diodes

Stefan Müller, Holger von Wenckstern, Florian Schmidt, Daniel Splith, Robert Heinhold, Martin Allen, and Marius Grundmann

Citation: Journal of Applied Physics **116**, 194506 (2014); doi: 10.1063/1.4901637
View online: https://doi.org/10.1063/1.4901637
View Table of Contents: http://aip.scitation.org/toc/jap/116/19
Published by the American Institute of Physics

Method of choice for fabrication of high-quality ZnO-based Schottky diodes

Stefan Müller,[1,a)] Holger von Wenckstern,[1] Florian Schmidt,[1] Daniel Splith,[1]
Robert Heinhold,[2] Martin Allen,[2] and Marius Grundmann[1]
[1]*Universität Leipzig, Institut für Experimentelle Physik II, Abteilung Halbleiterphysik, Linnéstraße 5, 04103 Leipzig, Germany*
[2]*The MacDiarmid Institute for Advanced Materials and Nanotechnology, University of Canterbury, Christchurch 8043, New Zealand*

(Received 4 September 2014; accepted 1 November 2014; published online 20 November 2014)

We present a comprehensive comparison of electrical properties of differently fabricated high quality Schottky contacts on ZnO thin films grown by pulsed laser deposition. Thermally evaporated Pd/ZnO Schottky contacts exhibit ideality factors as low as 1.06 due to their high lateral homogeneity. The effective Richardson constant determined using these homogeneous contacts is $(7.7 \pm 4.8)\,\mathrm{A\,cm^{-2}\,K^{-2}}$ close to the theoretical value of $32\,\mathrm{A\,cm^{-2}\,K^{-2}}$. However, their rectification ratio is at most five orders of magnitude due to their comparably small barrier height ($\approx$0.7eV). The largest effective barrier height (1.11 eV) and rectification ratio (7×10^{10}) was obtained for reactively sputtered PdO_x/ZnO Schottky contacts. Eclipse pulsed laser deposited IrO_x/ZnO Schottky contacts were found to combine very good lateral homogeneity ($n \approx 1.1$), with a reasonably large barrier height (0.96 eV) and large rectification ratio ($\approx$9 orders of magnitude). Our results for differently fabricated Schottky contacts suggest that the barrier formation is highly dependent on the presence of oxygen vacancies close to the interface and the different compensation mechanisms involved. © *2014 AIP Publishing LLC*.
[http://dx.doi.org/10.1063/1.4901637]

I. INTRODUCTION

Over the last 15 yr, ZnO has been the subject of renewed interest as a transparent semiconducting oxide (TSO). A significant part of this research has been focused on the use of ZnO to develop transparent electronics.[1,2] However, difficulties in obtaining high quality *p*-type ZnO have seriously hindered the development of bi-polar devices. Consequently, the spotlight has switched to unipolar devices such as Schottky diodes, UV photodetectors, and metal semiconductor field effect transistors, for which Schottky contacts (SCs) represent the key component.

The first report on SCs on vacuum cleaved ZnO bulk single crystals was published by Mead in 1965.[3] The fabrication of high-quality, reproducibly operating SCs, remained challenging until the last decade. In order to obtain device quality SCs on ZnO bulk single crystals various surface treatments were investigated. Especially, SCs fabricated on ZnO surfaces treated with oxygen plasma,[4,5] sulfide,[6] or hydrogen peroxide[7–9] showed improved properties compared to their counterparts on untreated surfaces. A major breakthrough in the development of SCs on untreated ZnO surfaces with remarkably low ideality factors and large effective barrier heights was achieved by Allen *et al.* in 2007. They reported reactively sputtered AgO_x/SCs on ZnO bulk single crystals with ideality factors close to unity (1.1).[10] Using such SCs with nearly homogeneous barriers, it was for the first time possible to extract an experimental value of the effective Richardson constant of ZnO of $10\,\mathrm{A\,cm^{-2}K^{-2}}$ from temperature dependent current-voltage (*I-V*) measurements[11] which is close to the theoretical value of $32\,\mathrm{A\,cm^{-2}K^{-2}}$. A further improvement of the barrier homogeneity of SCs on ZnO bulk single crystals was achieved using eclipse pulsed laser deposition (E-PLD) of noble metal in an oxygen atmosphere, resulting in metal oxide SCs involving IrO_x, PtO_x, or PdO_x.[12] The ideality factor of such contacts approaches the image-force controlled limit confirming their lateral homogeneity.

In this paper, we investigate the influence of fabrication methods, in particular, thermal evaporation, reactive sputtering, and E-PLD on the properties of Schottky barrier diodes ZnO thin films (TFs).

II. EXPERIMENTAL

For the present investigation, we used *c*-oriented ZnO thin films grown by pulsed laser deposition.[13,14] The thin films contained two functional zinc oxide layers. First, an approximately 50 nm thick, highly aluminium doped ZnO:Al layer was deposited on *a*-plane sapphire substrates. This highly conducting layer ($\rho \approx 10^{-3}\,\Omega\,\mathrm{cm}$) was used as an ohmic back-contact and ensures a low series resistance for the resulting Schottky diode.[15] Subsequently, an approximately 1 μm thick nominally undoped ZnO layer was grown. Both layers were deposited using identical growth conditions. The growth temperature was approximately 650 °C and the oxygen partial pressure was set to 0.016 mbar. The SCs were fabricated by three different techniques: thermal evaporation,[15] reactive sputtering,[16] and reactive E-PLD.[12] Planar, circular SCs were defined using photolithography. The diameters of the SCs range between 150 and 750 μm. The thermally evaporated SCs consisted of a 40 nm thick

a)Electronic mail: stefan.mueller@physik.uni-leipzig.de

Pd-layer. The sputtered SCs were made up of two different DC (direct current) sputtered layers. The first layer was PdO_x sputtered in a 1/1 vol. % Ar/O_2 atmosphere. Subsequently, a second Pd layer was sputtered in a pure argon atmosphere, which ensures an equipotential surface.[16] The total thickness was about 50 nm. The E-PLD grown SCs were ablated from a metallic Ir target at room temperature ($T = 293$ K) and an oxygen partial pressure of 0.13 mbar (10^{-1} Torr). A more precise description of the conditions used is given elsewhere.[12] The thickness of the IrO_x layer was approximately 50 nm. A sputtered Au capping layer with an approximate thickness of 50 nm was used to improve the lateral conductivity of the IrO_x SCs. The net-doping density of the thin films used for this investigation was $4 - 6 \times 10^{16}$ cm^{-3}.

All SCs were investigated by *I-V* measurements at room temperature. For selected SCs, we additionally performed *I-V* measurements in a temperature range between 20 K and 320 K or 293 K and 393 K, respectively. We also performed capacitance-voltage (*C-V*) measurements at room temperature for selected SCs using an *Agilent 4292A* precision impedance analyzer. The *I-V* characteristics were recorded using an *Agilent 4155C* semiconductor parameter analyzer. The room temperature and temperature dependent measurements up to 393 K were performed in a semiautomatic *Süss Waferprober system P 200*. The low temperature *I-V* measurements were recorded in a *CTI-CRYOGENICS Model 22* cryostat.

III. THEORY OF *I-V* CHARACTERISTICS

The current transport through ZnO SCs on our thin films can be described by thermionic emission.[17] Considering the series and parallel resistances R_s and R_p of SCs, we used

$$I = I_s \exp\left(\frac{e(V_A - IR_s)}{nk_BT}\right) \times \left(1 - \exp\left(\frac{-e(V_A - IR_s)}{k_BT}\right)\right) + \frac{V_A - IR_s}{R_p}, \quad (1)$$

for the determination of the effective barrier height $\Phi_{B,eff}$ and the ideality factor n. In Eq. (1), e is the elementary charge, V_A is the applied voltage, T is the absolute temperature, and k_B Boltzmann's constant. This model incorporates the voltage dependence of the barrier through the ideality factor n. The saturation current I_s is given by

$$I_s = A_0 A^* T^2 \exp\left(\frac{-\Phi_{B,eff}}{k_BT}\right), \quad (2)$$

where A^* is the Richardson constant $A^* = \frac{4\pi e k_B^2 m^*}{h^3}$, with a theoretical value of 32 A cm^{-2} K^{-2} (using $m_e^* = 0.27\, m_{e,0}$), A_0 is the contact area, and $\Phi_{B,eff}$ is the effective barrier height of the Schottky diode. Lateral fluctuations of the barrier potential, especially visible at low measuring temperatures have to be considered for the explanation of experimental *I-V* characteristics.[18,19] Here, we used a model assuming a Gaussian distribution of the barrier heights as proposed by Sachs[20] and later worked out by Werner and Güttler[21]

$$P(\Phi_{B,m})(V_A) = \frac{1}{\sigma(V_A)\sqrt{2\pi}} \times \exp\left(-\frac{(\Phi_{B,m}(V_A) - \Phi_B)^2}{2\sigma^2(V_A)}\right). \quad (3)$$

The assumption of a Gaussian barrier height distribution was experimentally verified for Au/Co/$GaAs_{67}P_{33}$ Schottky-contacts by ballistic electron emission microscopy measurements (lateral resolution of 1 nm) of Schottky contacts.[22,23] The distribution is characterized by a voltage-dependent standard deviation $\sigma^2(V_A) = \sigma^2(V_A = 0) + \rho_3 V_A$ and mean barrier height $\Phi_{B,m}(V_A) = \Phi_{B,m}(V_A = 0) + \rho_2 V_A$. Assuming that both parameters have a linear voltage dependence, the ideality factor is given by

$$n = \frac{1}{1 - \rho_2 + (e\rho_3/2k_BT)}. \quad (4)$$

The parameters ρ_2 and ρ_3 are assumed to be temperature independent. The barrier height is given by

$$\Phi_{B,eff} = \Phi_{B,m} - \frac{\sigma^2}{2k_BT}. \quad (5)$$

Equation (5) is commonly used in literature to determine the mean barrier height. For that a plot of the effective barrier vs. inverse temperature is extrapolated to $T^{-1} \to 0$ to obtain the mean barrier height.[24,25] However, this approach may cause an overestimation of the mean barrier height for the following reason. SCs that show nearly ideal behavior at room temperature and above, often show non-ideal behavior at low temperatures, as shown in Ref. 11 Fig. 5 (inset). This figure shows that the ideality factor decreases and the barrier height increases strongly from 50 K up to 300 K before both parameters saturate and remain constant for higher temperatures. In this high temperature regime, the effective barrier height coincides with the mean barrier height. In other words, for each laterally inhomogeneous Schottky barrier diode, there exists a temperature $T_{n_{if}}$ above which $\Phi_{B,eff}$ equals $\Phi_{B,m}$ and $n(T)$ equals the image force controlled ideality factor n_{if} ($\approx$1.02 for our samples). Therefore, we extrapolated our $\Phi_{B,eff}$ vs. T^{-1} data to the temperature for which n equals n_{if}. This temperature can be deduced from the n vs. T^{-1} data. For the diode, depicted in Fig. 6, the commonly used fitting procedure results in a mean barrier height of 1.83 eV, which is an overestimation of more than 30% compared to the value $\Phi_{B,m} = 1.37$ eV obtained from extrapolating to $T_{n_{if}}$.

IV. RESULTS AND DISCUSSION

A. Thermally evaporated Schottky contacts

First, we discuss the properties and characteristics of the thermally evaporated Pd/ZnO SCs. Figure 1(a) shows room temperature *I-V* characteristic of one of the best evaporated SCs. A slight increase of the current is visible in reverse bias direction. This is explained by the voltage-dependent image force lowering effect which reduces the apparent barrier height. The voltage dependence of the image force lowering effect can be seen in the inset of Fig. 1(a). The additional

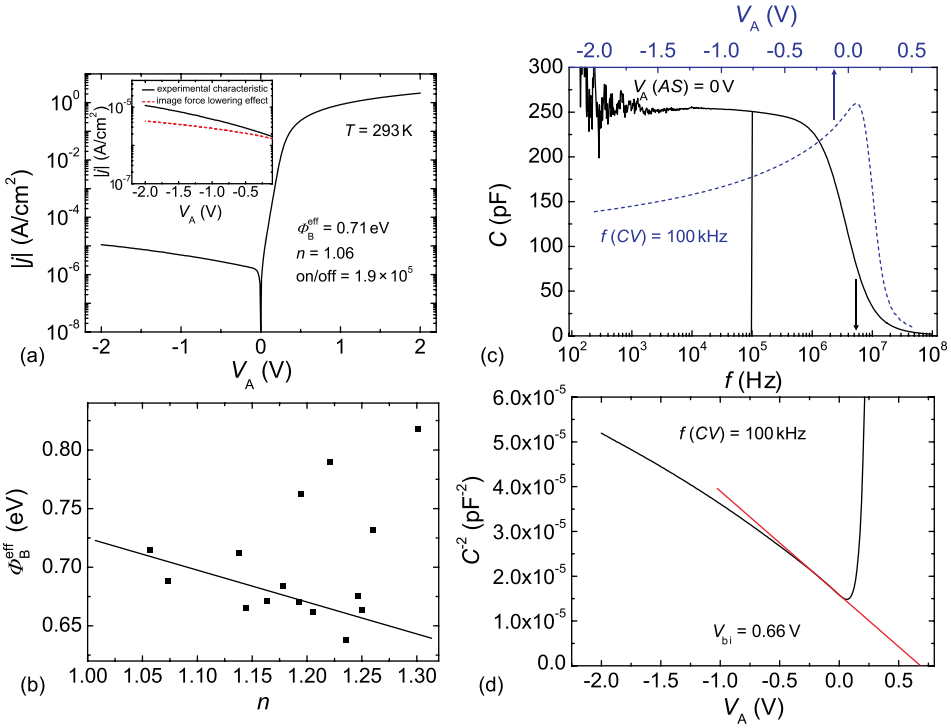

FIG. 1. (a) Room temperature *I-V* characteristic of one of the best thermally evaporated Pd/ZnO SC. The inset clarifies the effect of image force lowering on the reverse current. (b) Effective barrier height dependence on the ideality factor for all Pd/ZnO SCs of this sample. (c) Frequency- (lower axis) and voltage-dependent (upper axis) capacitance of the SC shown in (a). (d) C^{-2} dependence on the applied voltage determined from the capacitance measurement in (c).

excess current in the reverse direction is explained by lateral barrier height inhomogeneities introducing a voltage dependence, which will be thoroughly discussed for the sputtered SCs, for which their influence is more pronounced. In the forward direction, we observe a single exponential slope for voltages up to 0.25 V as expected for TE. For higher voltages, the SC is operating under flat band conditions. By fitting the exponential slope in the forward direction using TE the effective barrier height is 0.71 eV. The effective barrier height determined for our homogeneous SC agrees well with the value reported by Grossner *et. al.* (0.75 eV) for homogeneous Pd SCs ($n = 1.03$) fabricated by e-beam evaporation on ZnO bulk material.[26] In other reports on Pd SCs, the effective barrier height is also similar compared to our determined value.[15,27] However, the ideality factor of the SC reported here is significantly smaller. The ideality factor here is 1.06 close to unity, confirming the quality and homogeneity of PLD ZnO thin films and the thermally evaporated Pd SCs there on. The ideality factor reported here for the Pd/ZnO SCs is significantly smaller compared to previously reported values for SCs on our thin films.[15,16,27] It represents the lowest reported ideality factor for SCs on a ZnO thin film and comparable to that of SCs on ZnO bulk single crystals.[10–12] The small effective barrier of the evaporated SCs result in a relatively small rectification ratio of 1.9×10^5 of the SC depicted in Fig. 1(a). This rather small barrier height makes evaporated SCs uninteresting for devices. However, it is possible to use such SCs for the investigation of defects using capacitance-based spectroscopic methods.

Figure 1(c) shows the frequency- (lower axis) and voltage-dependent (upper axis) capacitance of the diode, as shown in Fig. 1(a). The frequency-dependent measurement shows that the cut-off frequency is above 1 MHz for our SCs due to the small series resistance. The voltage-dependent capacitance (*C-V*) was measured at 100 kHz to determine the mean barrier height. Extrapolating $C^{-2} \rightarrow 0$ (cf. Fig. 1(d)) yields a built-in voltage V_{bi} of 0.66 V. The barrier height was determined using

$$\Phi_{B,CV} = eV_{bi} + k_B T \ln\left(\frac{N_C}{N_D}\right) + k_B T, \tag{6}$$

where N_C is the conduction band edge density of states ($2.94 \times 10^{18}\,cm^{-3}$ at room temperature) and N_D is the net doping density. Using Eq. (6), a barrier height of 0.79 eV was extracted for the thermally evaporated SC. In Fig. 1, a slight bending of C^2 in dependence on the applied voltage is visible. The changing slope is due to an inhomogeneous net doping density caused by the in diffusion of Al from the ohmic back contact layer and the sapphire substrate, respectively. We used for our investigations comparably thick thin films (1 μm) to ensure a nearly constant net doping density in the surface near region. Therefore, only data points acquired close to the metal/semiconductor interface (in this case $-0.3\,V < V_A < 0\,V$) were considered for the extrapolation of the C^{-2} plot to zero. This reduces the potential error in the determination of the built-in potential induced by the doping gradient.

Figure 1(b) shows the dependence of the effective barrier height on the ideality factor for all thermally evaporated Pd SCs on one PLD ZnO film. We see that for most of the SCs the effective barrier height increases with decreasing ideality factor, as expected from Tung's theory.[28] However, some of the contacts are significantly above the main trend. For such SCs, the effective barrier height is unexpectedly large (0.73 eV–0.83 eV) given their relatively high ideality factor (1.2–1.3). In contrast to the other thermally evaporated SCs, a fitting of the forward bias current with TE yields a large deviation especially in the region just before the SCs are under flat band conditions. This means that, for these

SCs, the barrier formation mechanism is different compared to the typical evaporated SCs. Therefore, we have not used such SCs for further investigations. Note that the formation of such anomalous SCs which do not exhibit the expected linear behavior of effective barrier height vs. ideality factor is not unusual for the evaporated SCs investigated. Some of the anomalous contacts also exhibit a smaller current density compared to the normal SCs on the sample. One possible reason is that the geometrical area defined by photolithography does not agree with the electrical active area of the SC, e.g., due to photoresist residues or other contaminations on the sample. An overestimation of the active electrical area results in an overestimation of the effective barrier.

The SC depicted in Fig. 1(a) was additionally characterized at temperatures between 293 K and 358 K. This measurement was done some time after the measurement at room temperature, as shown in Fig. 1(a). This caused a slight deterioration in the room temperature properties. The thermally evaporated contacts were investigated up to a temperature of 358 K in order to prevent thermal degradation (usually starting for such kind of contacts around 360 K). Such irreversible changes in the *I-V* characteristics of evaporated SCs were already reported for ZnO based SCs.[29] The temperature dependent *I-V* characteristics are shown in Fig. 2(a). We see that the current increases for all voltages as expected for TE. In the reverse bias direction, the current is for temperatures up to 343 K, determined by image force lowering and barrier inhomogeneities. For the *I-V* characteristic measured at 358 K in the forward direction, a single exponential slope is visible for all investigated temperatures. The barrier height and ideality factor dependence on inverse temperature are shown in Figs. 2(b) and 2(c). Two different regions are visible indicated by the dashed guideline to the eye. For lower temperatures (293 K–313 K), we see a slight increase of the effective barrier height from 0.69 eV to 0.73 eV and a decrease of the ideality factor from 1.13 to 1.07. For temperatures above 313 K, the effective barrier height and ideality factor remain remarkably constant, apart some small fluctuations. Allen *et al*. demonstrated for homogeneous AgO_x/ZnO SCs on ZnO bulk single crystals that it is possible to determine an experimental value of the Richardson constant A^* ($10\,A\,cm^{-2}\,K^{-2}$) which is close to the theoretical value of $32\,A\,cm^{-2}\,K^{-2}$. The Richardson plot for our SC is depicted in Fig. 2(d). The increasing effective barrier height for temperatures below 313 K is also visible in the Richardson plot as a region of smaller slope. For larger temperatures, the slope increases, and a linear dependence is visible. The linear extrapolation of this region yields an experimental Richardson constant A^* of $(7.7\pm4.8)\,A\,cm^{-2}\,K^{-2}$ and a mean barrier height of $(0.69\,eV\pm0.03)\,eV$. The mean barrier height shows good agreement with the expected homogeneous barrier height, visualized by the trend-line in Fig. 1(b). Recently, Somvanshi and Jit reported an experimental value of the Richardson constant of $19.54\,Acm^{-2}K^{-2}$ (no error given) for Pd SCs on ZnO thin film.[30] However, this value was derived for a diode with a rectification ratio below 10^3 and an ideality factor above 2 at room temperature. Therefore, they had to use the modified Richardson plot including the barrier height distribution to achieve a reasonable value. We were able to determine a value close to the theoretical one without this approximation, which works for all SCs, due to the very good homogeneity of our SCs and ZnO thin films.

B. Eclipse pulsed laser deposition grown Schottky contacts

Figure 3(a) depicts the room temperature *I-V* characteristics of one of the best IrO_x/ZnO SCs. The IrO_x/ZnO SCs grown by E-PLD combine the homogeneity of Schottky barrier diodes (low ideality factor) realized by thermal evaporation with the very large rectification (large effective barrier

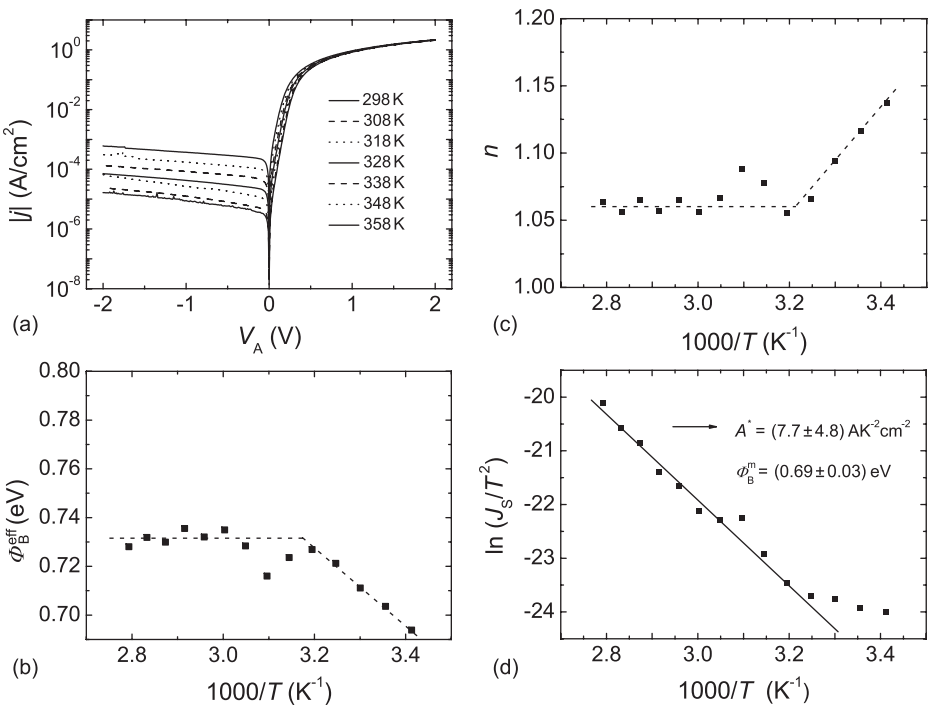

FIG. 2. (a) Temperature dependent *I-V* characteristics between 298 K and 358 K of the Pd/ZnO SC shown in Fig. 1(a); (b) effective barrier height and (c) ideality factor dependence on the inverse temperature determined from the measurement shown in (a); (d) Richardson plot of the Pd/ZnO SC.

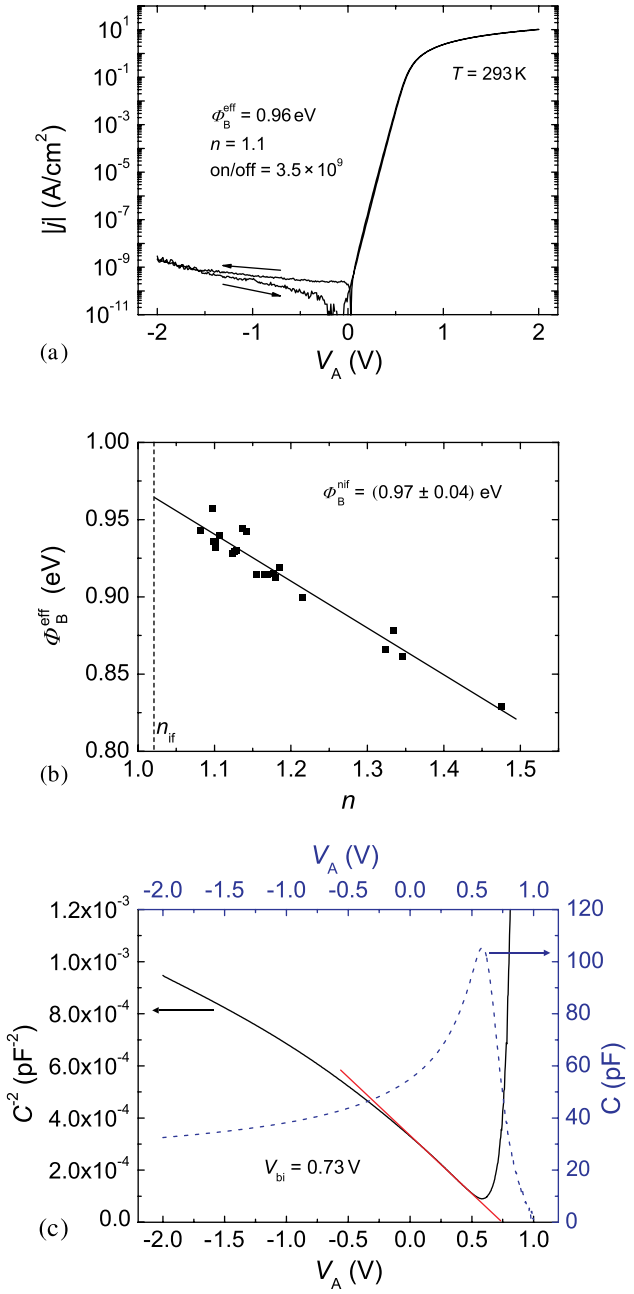

FIG. 3. (a) Room temperature *I-V* characteristic of one of the best IrO_x/ZnO SC fabricated by reactive eclipse pulsed laser deposition. The black arrow indicates the measurement direction. (b) Effective barrier height in dependence on the ideality factor of all IrO_x/ZnO SCs on this sample. (c) voltage-dependent (right axis) capacitance and the following C^{-2} dependence (left axis) of the SC shown in (a).

height) of the sputtered SCs (discussed in Sec. IV C). We observe a small hysteresis of the *I-V* characteristics in the reverse bias direction. The reverse current is generally smaller if the sweep direction is from negative to positive bias voltages. The direction of the respective measurement is indicated by the black arrows in Fig. 3(a). Differences between these measurements are greatest at small reverse voltages. The splitting of the zero current crossing for the two sweep directions is due to the charging and discharging current of an additional parallel capacitance caused, for example, by surface states. A similar behavior was also observed for a thermally evaporated Ag SC on Zn-polar bulk[31] and for a Pd SC on annealed O-polar ZnO bulk material.[8] We have already reported and discussed this behavior for SCs on PLD grown β-Ga_2O_3 thin films.[32] In the forward direction of the *I-V* characteristics, a single exponential slope over nine orders of magnitude up to 0.5 V is visible. The ideality factor determined is 1.1 close to that of the best evaporated SCs. The effective barrier height is 0.96 eV, much larger than that of the thermally evaporated Pd/ZnO SC depicted in Fig. 1(a), which results in a larger rectification ratio of 3.5×10^9. The effective barrier height dependence on ideality factor of all 22 working IrO_x SCs on the same ZnO sample is shown in Fig. 3(b). We observe again a linear dependence between both parameters. More than 80% of the investigated SCs have an ideality factor below 1.2 confirming the excellent homogeneity of this type of SC. The IrO_x Schottky barrier diodes on our PLD grown thin films have slightly higher ideality factors then those on bulk ZnO reported in Ref. 12 and the scatter in the Φ_B^{eff} versus *n*-plot is also larger. This is related to the inferior structural quality of our thin film compared to hydrothermal bulk ZnO single crystals from Tokyo Denpa. Such inhomogeneities are due to structural defects, which are of course present in higher densities in heteroepitaxial grown thin films compared to bulk single crystals. Another reason is also the small lateral temperature gradient over the sample during the PLD growth process, which also results in small lateral changes of crystalline quality and electron affinity across the sample. Variations in thin film homogeneity are also visible in a continuous change of the series resistance of the EPLD grown SCs, in this work (which all have the same dimensions) with position on the sample. The homogeneous barrier height for this sample is 0.97 eV.

The temperature dependent properties of the IrO_x/ZnO SCs were measured from 30 K to 320 K. For the low temperature measurements, the samples had to be mounted on a *TO23* using a gold and an epoxy resin which needs an additional curing step at 363 K for 45 min. The temperature dependent *I-V* measurement of the SC shown in Fig. 3(a) is depicted in Fig. 4(a) for temperatures between 50 K and 320 K. Note that the room temperature electrical properties of the SCs on the transistor socket are slightly deteriorated due to mounting compared to the sample just measured using the wafer prober. The ideality factor increased from 1.1 to 1.18 and the effective barrier decreased from 0.96 eV to 0.88 eV at room temperature. In the reverse direction, we see for all measured temperatures a current coinciding with the noise floor of the setup used. However, compared to the room-temperature measurements using the wafer prober the noise level in the cryostat is increased by 2 orders of magnitude. In the forward direction, the current again increases with increasing temperature as expected from TE. For temperatures below 260 K, a kink in the I-V characteristic is noticeable for small forward bias. This kink is again caused by barrier inhomogeneities. The ideality factor and effective barrier height dependence on inverse temperature determined from the results in Fig. 4(a) is shown in Figs. 4(b) and 4(c). The ideality factor strongly decreases with increasing temperature and approaches unity for high temperatures. The inset Fig. 4(b) shows the ideality factor for

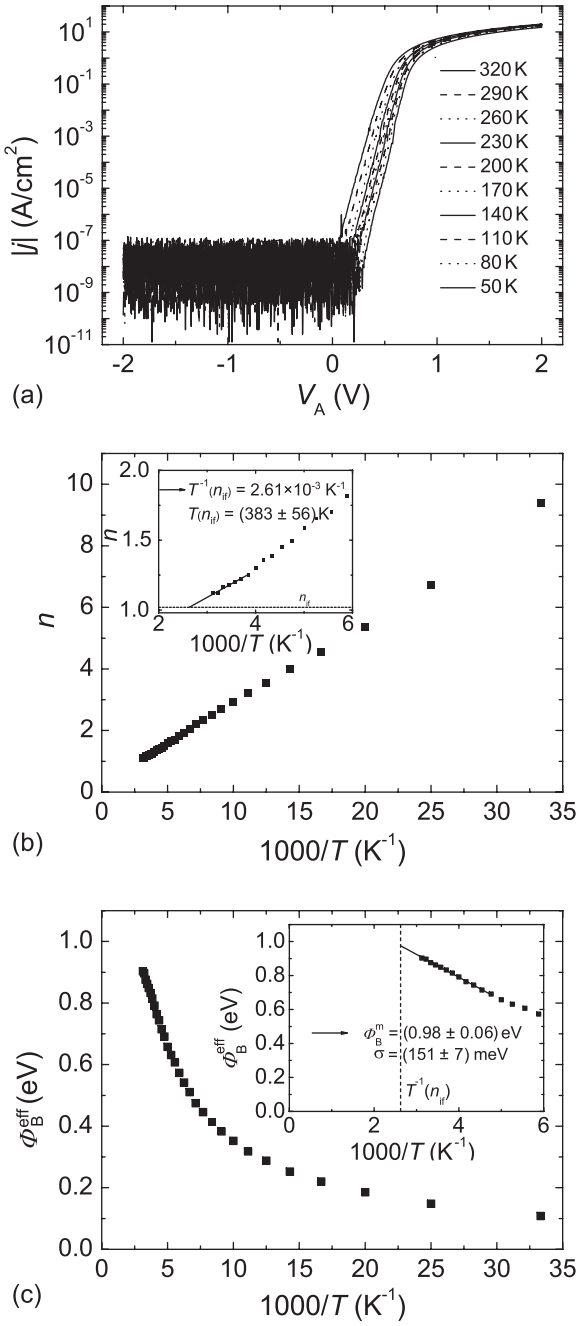

FIG. 4. (a) Temperature-dependent *I-V* characteristics between 50 K and 320 K of a IrO_x/ZnO SC fabricated by reactive eclipse pulsed laser deposition. (b) Ideality factor and (c) effective barrier height vs. inverse temperature of the SC shown in (a).

temperatures above 170 K. At high temperatures, we see a decrease of the slope of $n(T^{-1})$. By extrapolating this slope, we determined the temperature where the ideal image force controlled ideality factor is reached within this region to be $T_{\mathrm{nif}} = 383$ K, which as expected is lower than that for the reactively sputtered PdO_x/ZnO diode (cf. Sec. IV C). The use of this higher temperature region also has the advantage that the current transport is well described by TE and other possible transport mechanisms such as tunneling or trap-assisted tunneling can be safely ignored.[17] The barrier height also shows a strong dependence on the temperature. At low temperatures, we observe an increase of the effective barrier with increasing temperature. With increasing temperature the slope increases until the slope is linearly dependent on the inverse temperature for temperatures above 200 K. We used this region for the determination of the mean barrier height and standard deviation, which is for this SC (0.98 ± 0.06) eV and (151 ± 7) meV, respectively. Note that this mean barrier height is in very good agreement with the homogeneous barrier height of this sample. However, the mean barrier height determined by *C-V* measurements (cf. Fig. 3(c)) is with 0.87 eV smaller for the same SC.

C. Reactively sputtered Schottky contacts

We now consider the last fabrication technique for high quality Schottky contacts on ZnO which involves sputtered PdO_x/ZnO SCs. The room temperature *I-V* characteristic of one of the best sputtered PdO_x/ZnO SC is shown in Fig. 5(a). The reverse current is below the detection limit of the parameter analyser ($\sim 10^{-13}$ A). For small forward voltages ($V < 0.9$ V), an exponential increase is visible. At higher voltages, the diode is under flat band conditions. At small forward current, a second exponential slope is visible, which is caused by barrier height inhomogeneities. This effect for SCs fabricated on our thin films may be caused by Al_2O_3 particles in the ohmic back contact.[33] However, for this investigation, we used thin films with a quite thin ohmic back contact layer, therefore, it is more likely that this barrier height inhomogeneities are caused by lateral inhomogeneities of the sputtered PdO_x contact, e.g., varying oxidation state. The effective barrier height of the SC depicted in Fig. 5(a) is 1.11 eV, which is comparable to the best SCs on ZnO bulk single crystals[10–12] and the largest of the different techniques investigated. The ideality factor of the sputtered SCs is ≈1.3, which is the largest of the SCs investigated here. Tung explained an increasing ideality factor by a large number of nanoscale low barrier patches.[28] The sputtered SCs are fabricated in an Ar/O_2 atmosphere which causes oxidation of the Pd. The sputtering in this environment produces damaging ionized oxygen ions that are accelerated to the substrate and can cause barrier height inhomogeneities. This will be explained later in more detail. The ideality factor of the SC shown in Fig. 5(a) is 1.32, which was typical of the sputtered SCs on our thin films. The rectification ratio of the sputtered SCs due to the large effective barrier height was the largest of the investigated SCs. In the case of the SC depicted in Fig. 5(a), the rectification ratio is about 7×10^{10} and still limited by the noise floor of the parameter analyser used. This very large rectification ratio is similar to the best SC fabricated on ZnO bulk single crystals.[11,12] Figure 5(b) depicts a histogram of the rectification ratio of all 17 working SCs on this sample. The rectification ratio ranges from 5 to 11 orders of magnitude with an average of 8.1 orders of magnitude. The effective barrier height and ideality factor of all working SCs on this sample (17 contacts) are shown in Fig. 5(c). We highlight two regions with a linear dependence of the effective barrier height on the ideality factor, with different slopes. The point of intersection is approximately located at an ideality factor of 1.5 with a steeper slope for SCs with ideality factors less than this value. The linear dependence of the effective barrier height on the ideality factor

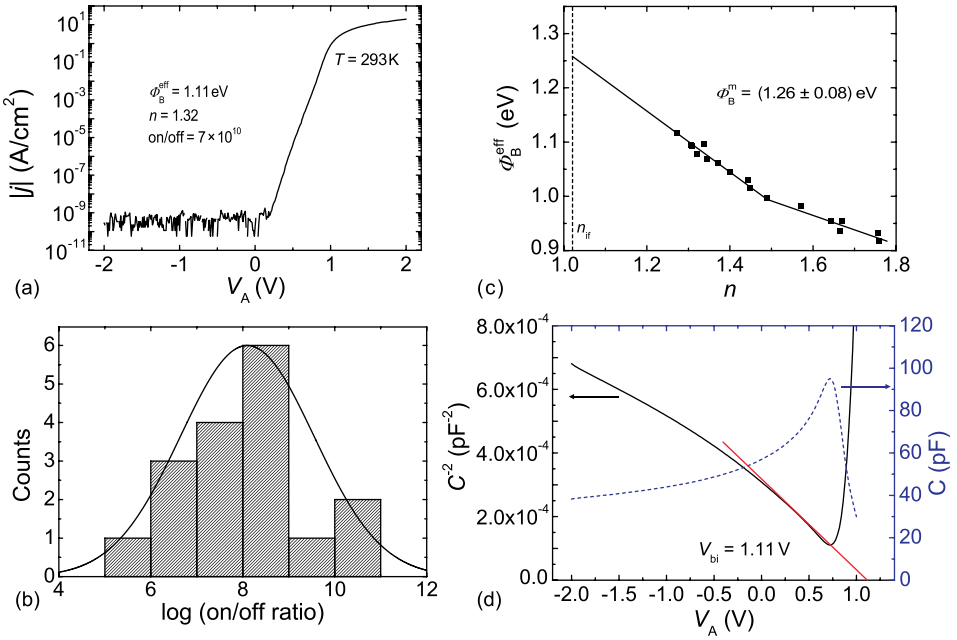

FIG. 5. (a) Room temperature *I-V* characteristic of one of the best PdO_x/ZnO SC. (b) Histogram of the rectification ratio $(I(V=2\,\mathrm{V})/I(V=-2\,\mathrm{V}))$ of all SCs on this sample. (c) Effective barrier height in dependence on the ideality factor for all PdO_x/ZnO SCs of this sample. (d) voltage-dependent (right axis) capacitance and the following C^{-2} dependence (left axis) of the SC shown in (a).

for SCs fabricated on the same sample is explained by Tung's theory of inhomogeneous SCs.[28] For small ideality factors (small density of nanoscale barrier inhomogeneities), the effective barrier height is proportional to the ideality factor, whereas for higher ideality factors (high density of nanoscale barrier inhomogeneities), it flattens to be a fixed value independent of the ideality factor.[34] Fitting the linear dependence of the effective barrier height for small ideality factors yields a homogeneous barrier height Φ_B^{nif} of 1.26 eV, which is in good agreement with a previous report for this type of SCs on PLD grown thin films.[33] The mean barrier height of 1.25 eV deduced from *C-V* measurement (cf. Fig. 5(d)) is in very good agreement with the homogeneous barrier height.

Figure 6(a) depicts the temperature dependent *I-V* characteristics of the sputtered SCs shown in Fig. 5(a). A high temperature induced irreversible degradation appears for the sputtered SCs for higher temperatures compared to the thermal evaporated SCs. Therefore, the temperature dependent *I-V* characteristics are recorded under ambient air conditions for temperatures ranging from 293 K to 393 K. The forward and reverse current increases with increasing temperature as expected for TE. In reverse direction, the increase in current can only be seen for temperatures above 333 K, for which the current is above the noise floor of the parameter analyser. Interestingly, the reverse current at 393 K is no longer determined by TE but instead an ohmic shunt resistance. With increasing temperature the second slope in the *I-V* characteristics visible for small V_A becomes less prominent; for $T \geq 393$ K only a single slope is visible. The dependence of the ideality factor and effective barrier height on the inverse temperature is shown in Figs. 6(b) and 6(c), respectively, with a linear dependence on T^{-1} for temperatures up to 373 K. The ideality factor decreases from 1.32 (293 K) to 1.17 (373 K), and the effective barrier height increases from 1.11 eV (293 K) to 1.25 eV (373 K). The ideality factor increases and effective barrier height decreases for temperatures above 373 K, which is caused by a reversible thermal degradation of this type of SCs on ZnO. By fitting the linear dependence of the ideality factor on inverse temperature we determined the temperature T_{nif}, for which the lowest theoretical ideality factor n_{if} is reached to be 471 K. Using this temperature, we determined the mean barrier height from Fig. 6(c) to be 1.37 eV with a standard deviation of 193 meV.

V. DISCUSSION OF THE RESULTS

The barrier heights of the differently fabricated SCs discussed in Sec. IV are summarized in Table I. For the thermally evaporated SCs, the barrier heights determined by *I-V* and *C-V*-measurements show good agreement. Compared to barrier heights of evaporated SCs reported so far, which are summarized in the first part of Table II, it is obvious that in several of the reports the SCs exhibit barrier heights similar to the results presented here, in the range between 0.6 eV and 0.7 eV independent of the metal used. The work function of the metals used for the different SCs is given in Table II (adapted from Refs. 35 and 36). It is well known from literature that structural, surface-near defects (e.g., oxygen vacancy (V_O)) close to the ZnO surface play an important role for the formation of ZnO SCs.[37,38] At the metal-ZnO interface, V_O is doubly ionized; the energy level of this V_O^{2+} transition is approximately 0.6 eV–0.7 eV below the conduction band minimum.[39–41] Therefore, Allen *et al.* attributed the comparably small barrier heights for evaporated SCs to an increased V_O density at the metal-semiconductor interface which leads to strong pinning of the surface Fermi level, resulting in barrier heights close to the V_O^{2+} energy level at 0.6 to 0.7 eV.[37] Such behavior is also a reasonable explanation for our thermally evaporated SCs and generally agrees very well with previous results on evaporated SCs.[4,26,31,42–47] Defects being potential candidates in the expected energy range were also reported as bulk defect. Such defects were generated by mechanical polishing,[29,43] proton irradiation,[48] or annealing.[49] SCs with barrier heights

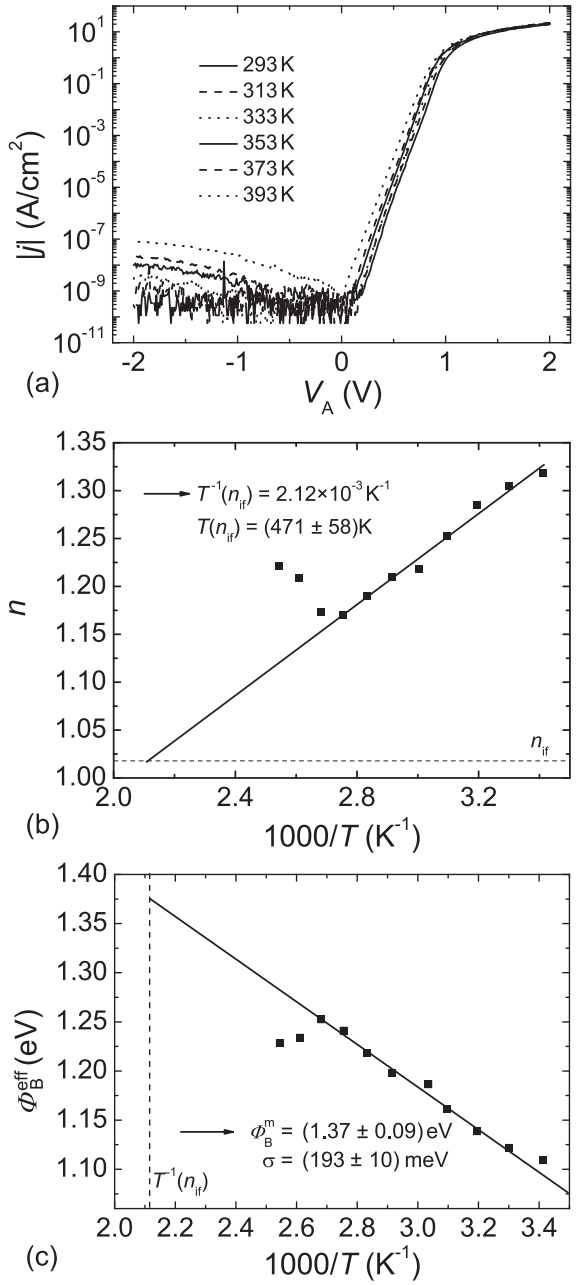

FIG. 6. (a) Temperature-dependent *I-V* characteristics between 293 K and 393 K of the sputtered PdO_x/ZnO SC shown in Fig. 5 (a). (b) Ideality factor and (c) effective barrier height in dependence on the inverse temperature determined from the measurement shown in (a).

which are larger than 0.7 eV were in most cases only achieved using surface oxidization treatments like oxygen plasma treatment or hydrogen peroxide.[8,46] A large density of surface defects 0.7 eV below the conduction band, as in our results, suggests that in the case of the thermally evaporated SCs, complete Fermi level pinning occurs. As a result, an upward band bending at the surface occurs independent of the metal used, which explains the small barrier heights of the evaporated SCs (cf. Fig. 7(a)).

The barrier heights of the E-PLD grown IrO_x SCs from *I-V* and *C-V*-measurements summarized in Table I show also a good agreement. The determined barrier heights are larger compared to the thermally evaporated Pd/ZnO SCs, although the work function and metal Miedema electronegativity of Ir

TABLE I. Determined barrier heights of SCs fabricate by thermal evaporation, reactive sputtering, and E-PLD. The barrier heights were determined by three different methods: dependence of the barrier height on the ideality factor of several SCs on one sample (Φ_B^{nif}), temperature dependent *I-V* measurement ($\Phi_{B,IVT}^{m}$), and *C-V* measurements ($\Phi_{B,CV}^{m}$(at 100 kHz)) of a single SC on this sample.

Preparation technique	Thermal evaporation (Pd)	Reactive sputtering (PdO_x)	Eclipse PLD (IrO_x)
Number of working contacts	15	17	22
Φ_B^{nif}	≈0.72 eV	1.26 eV	0.97 eV
$\Phi_{B,IVT}^{m}$	0.69 eV	1.37 eV	0.98 eV
$\Phi_{B,CV}$(at 100 kHz)	0.79 eV	1.25 eV	0.87 eV

are similar to that of Pd (cf. Table II and Ref. 50). Therefore, the increase of the mean barrier height of nearly 0.3 eV of the E-PLD grown SCs compared to the thermal evaporated SCs can not only be explained by changes in the work function and Miedema electronegativity. The results published so far for E-PLD grown SCs are summarized in the middle section of Table II. For these SCs no additional process, apart from the use of organic solvents (OS), was necessary. Reactively E-PLD grown SCs perform very well on both polar surfaces of ZnO bulk single crystals as well for SCs fabricated on our thin films. Allen *et al*. attributed this behavior to the partial oxidation of the SCs made of metals like Pd, Pt, or Ir and the compensation of surface V_O which interfere with Schottky barrier formation.[12] This behavior can be understood by considering the standard reduction potential E^0 at 298.15 K and 101.325 kPa of the noble metals Pd (0.951 V for $Pd^{2+} + 2e^- \rightleftharpoons Pd$), Pt (1.18 V for $Pt^{2+} + 2e^- \rightleftharpoons Pt$), and Ir (1.156 V for $Ir^{3+} + 3e^- \rightleftharpoons Ir$) all of which are larger than the standard reduction potential of Zn (−0.7618 V for $Zn^{2+} + 2e^- \rightleftharpoons Zn$).[51] When the noble metal oxide comes in contact with ZnO, Zn will reduce the noble metal oxide and will itself be oxidized. This results in a compensation of oxygen vacancies in the surface near region. It also explains why it is possible to fabricate high-quality noble metal oxide SCs on Zn- and O-terminated ZnO, while pure (non-oxidized) noble metal SCs with large barrier heights are only achieved on Zn-terminated ZnO bulk single crystals.[12] Comparing the mean barrier height of the E-PLD SCs with that of the sputtered SCs and thermally evaporated SCs shows that it is much larger than that of the thermally evaporated SCs but still 0.3 eV smaller than that of the sputtered SCs. The tentative explanation of the smaller mean barrier is that the additional oxygen at the interface due to the partial contact oxidation is able to compensate most of the oxygen vacancies in the ZnO and lift the Fermi-level pinning seen for the evaporated SCs. However, there is still a small upward band bending at the interface like that shown in Fig. 7(b).

The determined barrier heights for the reactively sputtered SCs in Table I show a good agreement as well. In comparison to the thermally evaporated and reactively E-PLD grown SCs, the barrier heights for these SCs are much larger. The literature results of reactively sputtered SCs summarized in the bottom section of Table II show that for this type of SCs no additional surface treatment, apart from cleaning

TABLE II. Properties of notable SCs on ZnO. The work function of the metals used for the evaporated SCs is given.[35,36] The effective barrier height Φ_B^{eff} and ideality factor n is given at room temperature determined by *I-V* measurements. The barrier height determined by *C-V* measurements Φ_B^{CV} is also summarized in column five if given in the corresponding report. In most of the reports, the rectification ratio was not given exactly. Therefore, we approximated them using the depicted *I-V* characteristics. If in a report several characteristics and corresponding effective barrier height and ideality factor are given only the values for the characteristic with the lowest ideality factor is given. The following abbreviations are used in the table: Thin film (TF), electron-beam evaporation (EBEV), thermal evaporation (TEV), vacuum evaporation (VEV), reactive sputtering (RS), direct current (DC), radio frequency (RF), (reactive) eclipse pulsed laser deposition ((R)E-PLD), metal organic chemical vapor deposition (MOCVD), plasma assisted molecular beam epitaxy (MBE), remote O_2/He Plasma cleaned (ROP), organic solvents (OS), phosphoric/hydrochloric acid (P/H acid), and boiling (boil.).

Material	Metal (W_m(eV))	Fabrication method	Surface treatment	$\Phi_{B,IV}^{eff}/\Phi_{B,CV}^{m}$ (eV)	n	Rectification ratio (± 2 V)	References
TF (MOCVD)	Ag (4.26 − 4.7)	EBEV	O_2 plasma	0.84/−	1.5	$\approx 10^5$ (at ± 1 V)	59
TF (MOCVD)	Ag	EBEV	Not reported	0.89/0.92	1.33	$\approx 10^6$ (at ± 1 V)	60
Bulk (Zn-polar)	Ag	VEV	OS	0.66/−	1.6	$\approx 10^3$ (at ± 1 V)	43
Bulk (Zn-polar)	Ag	EBEV	OS	1.02/1.0	1.2	$\approx 10^9$	31
Bulk (O-polar)	Ag	EBEV	OS	0.88/0.98	1.1	$\approx 10^7$	31
Bulk	Ag	TEV	OS	0.82/−	1.55	$\approx 10^3$ (at ± 1 V)	61
Bulk	Au (5.1)	TEV	P/H acid	0.66/0.67	1.05	Not shown	42
Bulk (O-polar)	Au	TEV	OS	−/−	1.19	$\approx 10^6$ (at ± 1 V)	62
Bulk (O-polar)	Au	EBEV	high/room T ROP	0.6/−	1.03	$\approx 10^7$	4
Bulk (Zn-polar)	Au	VEV	OS	0.67/−	1.6	$\approx 10^3$	43
Bulk (O-polar)	Au	EBEV	OS	0.69/0.7	1.1	$\approx 10^5$	31
Bulk (Zn-polar)	Au	EBEV	OS	0.71/0.7	1.4	$\approx 10^4$	31
Bulk (O-polar)	Au	TEV	OS/H_2O_2 (100 °C)	0.63/−	1.15	$\approx 10^7$	47
Bulk (O-polar)	Au	TEV/EBEV	OS/ROP	0.77/1.07	1.3	$\approx 10^5$	46
Bulk (Zn-polar)	Au	TEV/EBEV	OS/ROP	0.81/1.2	1.2	$\approx 10^6$	46
TF (MBE)	Au	EBEV	OS/H_2O_2 (100 °C)	1.19/−	1.15	$\approx 10^8$	63
Bulk (O-polar)	Ir (5.27)	TEV/EBEV	ROP	0.64/−	1.36	$\approx 10^8$	44
Bulk	Pd	TEV	P/H acid	0.6/0.61	1.05	Not shown	42
Bulk (O-polar)	Pd (5.12)	EBEV	OS	0.75/−	1.03	$\approx 10^5$	26
TF (PLD)	Pd	TEV	OS	0.81/1.14	1.49	$\approx 10^6$	15
Bulk (Zn-polar)	Pd	EBEV	OS	0.55/−	2.0	$\approx 10^2$	31
Bulk (O-polar)	Pd	EBEV	OS	0.59/0.59	1.2	$\approx 10^4$	31
Bulk (O-polar)	Pd	EBEV	OS/H_2O_2	1 − 1.2	1.8	$\approx 10^9$	8
Bulk (Zn-polar)	Pd	TEV/EBEV	OS/ROP	0.53/0.73	1.3	$\approx 10^3$	46
Bulk (O-polar)	Pd	TEV/EBEV	OS/ROP	0.61/0.68	1.2	$\approx 10^4$	46
Bulk (O-polar)	Pd	EBEV	OS/H_2O_2	−/0.6	1.4 − 2.1	$\approx 10^7$	9
TF (PLD)	Pd	TEV	OS	0.71/0.79	1.06	1.9×10^5	This work
Bulk (O-polar)	Pt (5.3 − 5.65)	EBEV	Boil. $(NH_4)_2S_x$	0.79/−	1.51	$\approx 10^5$	7
Bulk (Zn-polar)	Pt	EBEV	Boil. H_2O_2	0.89/0.93	1.15	$\approx 10^5$ (at ± 1 V)	6
Bulk (O-polar)	Pt	EBEV	OS	0.68/0.72	1.2	$\approx 10^5$	31
Bulk (Zn-polar)	Pt	EBEV	OS	0.55/−	2.0	$\approx 10^2$	31
Bulk (O-polar)	Pt	EBEV	OS/laser treated	0.73/0.85	1.77	$\approx 10^5$	45
Bulk (Zn-polar)	Ag	E-PLD	OS	0.73/−	1.01	Not shown	50
Bulk (Zn-polar)	Au	E-PLD	OS	0.57/−	<1.2	not shown	50
Bulk (Zn-polar)	Au	E-PLD	OS	0.82/−	<1.02	Not shown	50
Bulk (Zn-polar)	Ir	E-PLD	OS	1.0/−	<1.01	Not shown	50
Bulk (O-polar)	Ir	RE-PLD	OS	0.88/−	<1.01	$\approx 10^7$	12
Bulk (Zn-polar)	Ir	RE-PLD	OS	1.14/−	1.01	$\approx 10^9$	12
TF (PLD)	Ir	REPLD	OS	0.96/0.87	1.1	3.5×10^9	This work
Bulk (O-polar)	Pd	RE-PLD	OS	0.89/−	1.02	Not shown	12
Bulk (Zn-polar)	Pd	RE-PLD	OS	1.1/−	<1.01	Not shown	12
Bulk (Zn-polar)	Pd	E-PLD	OS	0.96/−	<1.03	Not shown	50
Bulk (O-polar)	Pt	RE-PLD	OS	0.98/−	<1.01	Not shown	12
Bulk (Zn-polar)	Pt	EP-LD	OS	1.08/−	<1.03	Not shown	50
Bulk (Zn-polar)	Pt	RE-PLD	OS	1.2/−	<1.01	Not shown	12
Bulk (Zn-polar)	Ru	E-PLD	OS	0.91/−	1.04	Not shown	50
TF (PLD)	Ag	RS (DC)	OS	0.66/1.35	1.57	$\approx 10^4$	16
TF (PLD)	Au	RS (DC)	OS	0.69/1.22	1.36	$\approx 10^4$	16
Bulk (O-polar)	Ag	RS (RF)	OS	0.99/0.97	1.06	$\approx 10^9$	64
Bulk (Zn-polar)	Ag	RS (RF)	OS	1.11/1.08	1.08	$\approx 10^9$	64
Bulk (O-polar)	Ag	RS (RF)	OS	0.99/1.06	1.04	$\approx 10^8$	10
Bulk (Zn-polar)	Ag	RS (RF)	OS	1.2/1.2	1.03	$\approx 10^9$	10

TABLE II. (*Continued.*)

Material	Metal (W_m(eV))	Fabrication method	Surface treatment	$\Phi^{eff}_{B,IV}/\Phi^{m}_{B,CV}$ (eV)	n	Rectification ratio (±2 V)	References
Bulk (Zn-polar)	Ag	RS (RF)	OS	≈1.16/−	1.09	$\approx 10^{10}$	12
TF (PLD)	Pd	RS (DC)	OS	0.73/1.2	1.25	$\approx 10^{4}$	16
TF (PLD)	Pd	RS (DC)	OS	1.11/1.25	1.32	7×10^{10}	This work
TF (PLD)	Pt	RS (DC)	OS	0.84/1.34	1.59	$\approx 10^{5}$	16

with organic solvents, is necessary to achieve high quality SCs, independent of the sputtering technique used for contact fabrication. As previously mentioned, the DC sputtered SCs are fabricated by reactive sputtering in a mixed Ar/O_2 atmosphere. Besides Ar atoms which are ionized to Ar^+ oxygen atoms are also ionized. Therefore, a reverse sputtering process of negatively charged ionized oxygen atoms impinging on the ZnO thin film occurs, which can be thought of an *in-situ* oxygen treatment of the ZnO surface at the beginning of the sputtering process. Such a treatment is likely to compensate surface near defects such as V_O or remove any surface electron accumulation layer (SEAL). This makes the fabrication of Schottky contacts using reactive sputtering also interesting for other oxides, where the Schottky barrier formation is complicated through surface contamination or a SEAL, for example, in In_2O_3[52] or SnO_2.[53,54] Recently, it was demonstrated, that even on In_2O_3 this reactive sputtering approach produces rectifying Schottky barrier diodes.[55] Further improvement in the Schottky barrier formation of reactively sputtered contacts on ZnO occurs due to the partial oxidation of the metal as discussed for the E-PLD grown SCs. The reduction of a noble metal oxide near the surface will also explain recent results that the first 1–2 nm at the interface of sputtered metal oxide SCs are not oxidized as determined by depth dependent hard X-ray photoelectron spectroscopy.[56] Therefore, we expect for the sputtered SCs a homogeneous energy distribution of surface defects due to compensation of oxygen vacancies by the additional oxygen of the oxidized SCs and the oxygen ions impinging on the thin film at the beginning of the sputtering process like shown in Fig. 7(c). For this homogeneous distribution no band bending will occur at the surface resulting in SCs with a homogeneous barrier height predicted by Schottky-Mott theory as for our sputtered PdO_x SCs (assuming the work function of Pd to be 5.12 eV (Ref. 57) and an electron affinity of 3.7 eV for ZnO (Ref. 58)). Summarizing, reactive sputtering allows fabrication of SCs with large barrier heights and large rectification ratios compared to evaporated SCs, making it a reasonable fabrication technique for electronics based on semiconducting oxides. Furthermore, reactive sputtering is a suitable technique for the fabrication of SCs on other materials, for which barrier formation is adversely affected by surface contaminants.

VI. CONCLUSIONS

In conclusion, we compared room-temperature and temperature dependent properties of high quality SCs on PLD grown thin films. The different SC fabrication methods considered were reactively sputtered PdO_x, thermally evaporated Pd, and E-PLD grown IrO_x. Some of the thermally evaporated Pd/ZnO SCs exhibit an excellent homogeneity ($n < 1.1$). However, the effective barrier height and consequently the rectification ratio is the smallest for such contacts. In contrast, the best sputtered PdO_x/ZnO SCs have large effective barrier heights (≈1.1 eV) and excellent rectification ratios of up to 10^{11}. The ideality factor of these sputtered SCs is determined by sputtering inhomogeneities and was relatively high up to 1.3. The E-PLD grown IrO_x/ZnO SCs are overall the best SCs investigated since they combine the good barrier homogeneity ($n \approx 1.1$) and large effective barrier height (Φ^{eff}_B close to 1 eV). The temperature-dependent measurements for all three kinds of SCs showed a behavior as expected for current transport controlled by

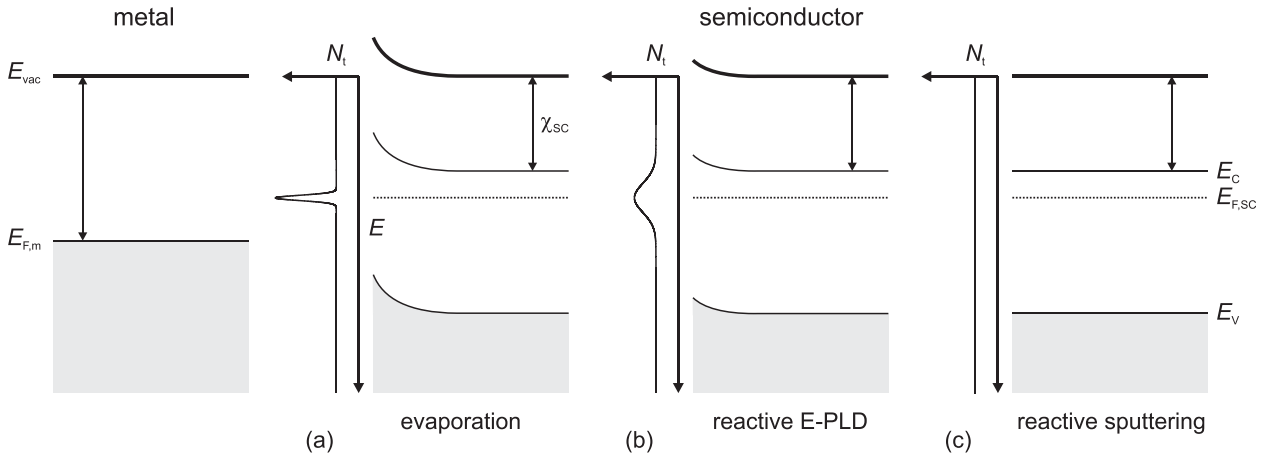

FIG. 7. Schematic band diagram of a metal and semiconductor without contact for (a) an unpinned Fermi level, (b) pinned Fermi level, and (c) a fully pinned Fermi level at the surface.

thermionic emission. We showed that with the best evaporated SCs, it is possible to determine an experimental value of the Richardson constant ($7.7 \pm 4.8\,A\,cm^{-2}\,K^{-2}$) for ZnO which is close to the theoretical value of $32\,A\,cm^{-2}\,K^{-2}$. The E-PLD and sputtered SCs showed a temperature dependent behavior as expected for Schottky contacts having a laterally varying barrier potential. For these contact types, we see an agreement of the homogeneous barrier determined at room temperature and the mean barrier height determined by temperature dependent measurements. Our results suggest a barrier formation which is highly determined by the concentration of near-surface oxygen vacancies. The thermally evaporated SCs are characterized by strong Fermi level pinning 0.7 eV below the conduction band which is attributed to oxygen vacancies explaining the comparatively small barrier heights. For the E-PLD grown IrO_x, we expect a partial compensation of these oxygen vacancies due to the reducing effect of the Zn atoms in the ZnO film on the noble metal oxide layer close to the SC interface which results in oxidation of the ZnO. The oxygen vacancies are fully compensated in sputtered SCs due to a combination of this oxidizing effect and additional oxidation due to oxygen ions in the plasma impinging on the ZnO surface at the beginning of the sputtering process in the mixed Ar/O atmosphere.

ACKNOWLEDGMENTS

This work has been supported by the Deutsche Forschungsgemeinschaft in the framework of Sonderforschungsbereich 762 "Functionality of Oxidic Interfaces" and the EFRE (SAB 100132251). We gratefully thank H. Hochmuth for PLD growth of the investigated samples, G. Ramm for the preparation of ZnO targets, M. Hahn and Z. Zhang for the preparation of the Schottky contacts.

[1]E. Fortunato, P. Barquinha, and R. Martins, Adv. Mater. **24**, 2945 (2012).
[2]H. Frenzel, A. Lajn, and M. Grundmann, Phys. Status Solidi RRL **7**, 605 (2013).
[3]C. Mead, Phys. Lett. **18**, 218 (1965).
[4]B. J. Coppa, R. F. Davis, and R. J. Nemanich, Appl. Phys. Lett. **82**, 400 (2003).
[5]H. L. Mosbacker, Y. M. Strzhemechny, B. D. White, P. E. Smith, D. C. Look, D. C. Reynolds, C. W. Litton, and L. J. Brillson, Appl. Phys. Lett. **87**, 012102 (2005).
[6]S.-H. Kim, H.-K. Kim, and T.-Y. Seong, Appl. Phys. Lett. **86**, 022101 (2005).
[7]S.-H. Kim, H.-K. Kim, and T.-Y. Seong, Appl. Phys. Lett. **86**, 112101 (2005).
[8]R. Schifano, E. V. Monakhov, U. Grossner, and B. G. Svensson, Appl. Phys. Lett. **91**, 193507 (2007).
[9]R. Schifano, E. V. Monakhov, B. G. Svensson, and S. Diplas, Appl. Phys. Lett. **94**, 132101 (2009).
[10]M. W. Allen, S. M. Durbin, and J. B. Metson, Appl. Phys. Lett. **91**, 053512 (2007).
[11]M. Allen, X. Weng, J. M. Redwing, K. Sarpatwari, S. Mohney, H. Von Wenckstern, M. Grundmann, and S. M. Durbin, IEEE Trans. Electron Devices **56**, 2160 (2009).
[12]M. W. Allen, R. J. Mendelsberg, R. J. Reeves, and S. M. Durbin, Appl. Phys. Lett. **94**, 103508 (2009).
[13]E. M. Kaidashev, M. Lorenz, H. von Wenckstern, A. Rahm, H.-C. Semmelhack, K.-H. Han, G. Benndorf, C. Bundesmann, H. Hochmuth, and M. Grundmann, Appl. Phys. Lett. **82**, 3901 (2003).
[14]M. Lorenz, H. Hochmuth, C. Grüner, H. Hilmer, A. Lajn, D. Spemann, M. Brandt, J. Zippel, R. Schmidt-Grund, H. von Wenckstern, and M. Grundmann, Laser Chem. **2010**, 140976.
[15]H. von Wenckstern, G. Biehne, R. A. Rahman, H. Hochmuth, M. Lorenz, and M. Grundmann, Appl. Phys. Lett. **88**, 092102 (2006).
[16]A. Lajn, H. v. Wenckstern, Z. Zhang, C. Czekalla, G. Biehne, J. Lenzner, H. Hochmuth, M. Lorenz, M. Grundmann, S. Wickert, C. Vogt, and R. Denecke, J. Vac. Sci. Technol. B **27**, 1769–1773 (2009).
[17]A. Lajn, H. von Wenckstern, M. Grundmann, G. Wagner, P. Barquinha, E. Fortunato, and R. Martins, J. Appl. Phys. **113**, 044511 (2013).
[18]H. C. Torrey and C. A. Whitmer, *Crystal Rectifiers*, 1st ed., edited by L. N. Ridenour and G. B. Collins (McCray-Hill, New York, 1948), Vol. 15, pp. 87–90; see http://www.jlab.org/ir/MITSeries.html.
[19]V. A. Johnson, R. N. Smith, and H. J. Yearian, J. Appl. Phys. **21**, 283 (1950).
[20]R. G. Sachs, Phys. Rev. **69**, 674 (1946).
[21]J. H. Werner and H. H. Güttler, J. Appl. Phys. **69**, 1522 (1991).
[22]A. Olbrich, J. Vancea, F. Kreupl, and H. Hoffmann, Appl. Phys. Lett. **70**, 2559 (1997).
[23]A. Olbrich, J. Vancea, F. Kreupl, and H. Hoffmann, J. Appl. Phys. **83**, 358 (1998).
[24]S. Acar, S. Karadeniz, N. Tuğluoğlu, A. Selçuk, and M. Kasap, Appl. Surf. Sci. **233**, 373 (2004).
[25]H. Wenckstern, S. Weinhold, G. Biehne, R. Pickenhain, H. Schmidt, H. Hochmuth, and M. Grundmann, *Advances in Solid State Physics*, Advances in Solid State Physics, Vol. 45, edited by B. Kramer (Springer, Berlin Heidelberg, 2006), pp. 263–274.
[26]U. Grossner, S. Gabrielsen, T. M. Borseth, J. Grillenberger, A. Y. Kuznetsov, and B. G. Svensson, Appl. Phys. Lett. **85**, 2259 (2004).
[27]H. von Wenckstern, E. M. Kaidashev, M. Lorenz, H. Hochmuth, G. Biehne, J. Lenzner, V. Gottschalch, R. Pickenhain, and M. Grundmann, Appl. Phys. Lett. **84**, 79 (2004).
[28]R. T. Tung, Phys. Rev. B **45**, 13509 (1992).
[29]A. Y. Polyakov, N. B. Smirnov, E. A. Kozhukhova, V. I. Vdovin, K. Ip, D. P. Norton, and S. J. Pearton, J. Vac. Sci. Technol., A **21**, 1603 (2003).
[30]D. Somvanshi and S. Jit, IEEE Electron Device Lett. **34**, 1238 (2013).
[31]M. W. Allen, M. M. Alkaisi, and S. M. Durbin, Appl. Phys. Lett. **89**, 103520 (2006).
[32]D. Splith, S. Müller, F. Schmidt, H. von Wenckstern, J. J. van Rensburg, W. E. Meyer, and M. Grundmann, Phys. Status Solidi A **211**, 40 (2014).
[33]S. Müller, H. von Wenckstern, O. Breitenstein, J. Lenzner, and M. Grundmann, IEEE Trans. Electron Devices **59**, 536 (2012).
[34]R. Schmitsdorf and W. Mönch, Eur. Phys. J. B **7**, 457 (1999).
[35]E. H. Rhoderick and R. H. Williams, *Metal-Semiconductor Contacts* (Oxford Science, Oxford, 1988), pp. 48–89.
[36]M. Grundmann, *The Physics of Semiconductors* (Springer-Verlag, 2006), pp. 401–425.
[37]M. W. Allen and S. M. Durbin, Appl. Phys. Lett. **92**, 122110 (2008).
[38]L. J. Brillson and Y. Lu, J. Appl. Phys. **109**, 121301 (2011).
[39]C. G. Van de Walle, Physica B **308**, 899 (2001).
[40]F. A. Selim, M. H. Weber, D. Solodovnikov, and K. G. Lynn, Phys. Rev. Lett. **99**, 085502 (2007).
[41]A. Boonchun and W. R. L. Lambrecht, Phys. Status Solidi B **250**, 2091 (2013).
[42]R. C. Neville and C. A. Mead, J. Appl. Phys. **41**, 3795 (1970).
[43]A. Y. Polyakov, N. B. Smirnov, E. A. Kozhukhova, V. I. Vdovin, K. Ip, Y. W. Heo, D. P. Norton, and S. J. Pearton, Appl. Phys. Lett. **83**, 1575 (2003).
[44]L. J. Brillson, H. L. Mosbacker, M. J. Hetzer, Y. Strzhemechny, G. H. Jessen, D. C. Look, G. Cantwell, J. Zhang, and J. J. Song, Appl. Phys. Lett. **90**, 102116 (2007).
[45]M.-S. Oh, D.-K. Hwang, J.-H. Lim, Y.-S. Choi, and S.-J. Park, Appl. Phys. Lett. **91**, 042109 (2007).
[46]Y. Dong, Z.-Q. Fang, D. C. Look, G. Cantwell, J. Zhang, J. J. Song, and L. J. Brillson, Appl. Phys. Lett. **93**, 072111 (2008).
[47]Q. L. Gu, C. K. Cheung, C. C. Ling, A. M. C. Ng, A. B. Djurisic, L. W. Lu, X. D. Chen, S. Fung, C. D. Beling, and H. C. Ong, J. Appl. Phys. **103**, 093706 (2008).
[48]F. D. Auret, S. A. Goodman, M. Hayes, M. J. Legodi, H. A. van Laarhoven, and D. C. Look, Appl. Phys. Lett. **79**, 3074 (2001).
[49]V. Quemener, L. Vines, E. V. Monakhov, and B. G. Svensson, Appl. Phys. Lett. **100**, 112108 (2012).
[50]M. W. Allen and S. M. Durbin, Phys. Rev. B **82**, 165310 (2010).
[51]P. Vanysek, *Electrochemical Series in CRC Handbook of Chemistry and Physics, Internet Version*, edited by D. R. Lide (CRC Press, Boca Raton, FL, 2005), pp. (8–23)–(8–33).

[52]O. Bierwagen, J. S. Speck, T. Nagata, T. Chikyow, Y. Yamashita, H. Yoshikawa, and K. Kobayashi, Appl. Phys. Lett. **98**, 172101 (2011).
[53]E. D. Frasart, J. Darville, and J. Gilles, Surf. Sci. **126**, 518 (1983).
[54]J. Szuber, G. Czempik, R. Larciprete, D. Koziej, and B. Adamowicz, Thin Solid Films **391**, 198 (2001).
[55]H. von Wenckstern, D. Splith, F. Schmidt, M. Grundmann, O. Bierwagen, and J. S. Speck, APL Mater. **2**, 046104 (2014).
[56]A. Lajn, H. von Wenckstern, M. Grundmann *et al.* "Are noble metal oxide-oxide semiconductor diodes Schottky diodes?" (unpublished).
[57]B. Nieuwenhuys, R. Bouwman, and W. Sachtler, Thin Solid Films **21**, 51 (1974).
[58]K. Jacobi, G. Zwicker, and A. Gutmann, Surf. Sci. **141**, 109 (1984).
[59]S. Liang, H. Sheng, Y. Liu, Z. Huo, Y. Lu, and H. Shen, J. Cryst. Growth **225**, 110 (2001).
[60]H. Sheng, S. Muthukumar, N. W. Emanetoglu, and Y. Lu, Appl. Phys. Lett. **80**, 2132 (2002).
[61]E. Gür, S. Tüzemen, B. Kiliç, and C. Coşkun, J. Phys.: Condens. Matter **19**, 196206 (2007).
[62]F. D. Auret, S. A. Goodman, M. J. Legodi, W. E. Meyer, and D. C. Look, Appl. Phys. Lett. **80**, 1340 (2002).
[63]E. Gür, G. Tabares, A. Arehart, J. M. Chauveau, A. Hierro, and S. A. Ringel, J. Appl. Phys. **112**, 123709 (2012).
[64]M. W. Allen, P. Miller, R. J. Reeves, and S. M. Durbin, Appl. Phys. Lett. **90**, 062104 (2007).